BU-1640-M

Mathematical Models for Photoreceptor Interactions

Miguel Angel Colón Vélez
UNIVERSITY OF PUERTO RICO - HUMACAO
Daniel Jesus Hernández
BOSTON UNIVERSITY
Ubaldo Rodríguez Bernier
UNIVERSITY OF PUERTO RICO - CAYEY
Jon Van Laarhoven
LAWRENCE UNIVERSITY
Erika Camacho
LOS ALAMOS NATIONAL LABORATORY

December 12, 2003

Abstract

The retina is arguably the single most important component in the vision process. Via its photoreceptors it is responsible for converting electromagnetic radiation into a chemical signal understandable by the brain. The interactions between rods and cones in the retina have been the focus of innumerable experimental and theoretical biological studies in previous decades, yet the understanding of these interactions is still in its infancy. We develop mathematical models which address the possibilities of direct photoreceptor interactions through horizontal cells as well as indirect interactions via an intermediary trophic factor. We address the role these means of communication play in the presence of the degenerative disease, Retinitis pigmentosa. The diseased system is reduced by considering the rod-cone interaction mechanism in the physiology of a disease free person. Extensive analyses of the dynamics of the nonhyperbolic solutions of the models (with and without delay) are offered. We show the disease free system exhibits a *fold-Hopf bifurcation.* Biological interpretation of all systems is given with the long-term objective of using our results to aid in prevention of vision loss in retinally degenerative diseases.

1 Introduction

> *To excite in us tastes, odors, and sounds I believe that nothing is required in external bodies except shapes, numbers, and slow or rapid movements. ...if ears, tongues, and noses were removed, shapes and numbers and motions would remain, but not odors or tastes or sounds.* -Galileo Galilei [18]

Vision is the most far reaching of the five senses; through vision we obtain information about the most distant objects in our world, as well as knowledge of worlds unknown. The eye has been the subject of inquisition for hundreds of years, its function ever more exposed by man's inquisitive eye. Our understanding of the form and function of the eye has advanced by leaps and bounds, yet every answer begs more questions. While our knowledge reaches farther than ever, the number of questions about this fascinating organ is literally unbounded.

Of the plethora of current unanswered questions, many involve the interactions between photoreceptors: the cells which convert light to chemical signals. Some is known, more is postulated, and biologists work diligently to understand the intercellular and extracellular means by which photoreceptors interact. Bearing an alternative tool to the microscope, we join our colleagues in exploration of the eye. Through mathematics we hope to increase knowledge of the relationship between rods and cones in the human retina, and in so doing cast light on the marvelous sense of sight and aid in preservation of vision amidst disease.

1.1 How the Eye Processes Light

The images of the world around us are captured by the eye through a series of complex steps. The eye must detect, transduce, and process light signals before sending them to the brain (for interpretation) via the optic nerves. Utilizing over a billion specialized light sensitive photopigments molecules, the eye detects light photons of various wavelengths. After light stimuli is absorbed, it must be converted into electrical signals on the cell membrane. In other words the light input must be converted into information that can be read by the nervous system. Light signals must be filtered (processed)

before transmission to the brain[7] [16].

Every component of the eye takes part in the visual process, but some structures play a more important role than others. Following Sherwood's description of the eye physiology, we briefly describe some of the various components of the eye and their roles in the visual cascade[16]. Light enters through the cornea, the transparent layer covering the eye. The cornea contributes most extensively to the eye's refractive ability; the other structure important to the eye's refractive power is the lens. The light then passes through the pupil, the round opening in the center of the iris. The iris is responsible for eye color and for controlling the amount of light that enters the eye. Through muscle contractions it can adjust its size to admit more or less light as needed. In bright light the circular muscles contract causing the pupil to get smaller and reduce the amount of light entering the eye. On the other hand, the radia muscles contract in the dark causing the pupil to dilate and allow the entrance of more light. After passing through the pupil, light passes to the lens and then through the vitreous humor (the larger posterior cavity between the lens and the retina)[16]. Contraction of the ciliary bodies allows the lens to focus images on the retina. Finally, light contacts the retina, the inner most coat under the choroid. The choirod is responsible for supplying blood to the eye[8]. The white of the eye is known as the sclera and it forms "part of the supporting wall of the eye ball"[8]. The retina consists of an outer pigmented layer and inner nervous tissue layer and more importantly, it contains the rods and cones: the photoreceptors that convert light energy into nerve impulses that are sent to the brain. Unlike other receptors, light absorption hyperpolarizes (inhibits) the photoreceptors. It is in the dark that these cells are depolorized (activated)[16].

Absorption of light leads to a cascade of biochemical events triggered by the activation of the photopigments. When a photopigment absorbs light it dissociates its retinene and opsin components. Its retinene portion, identical in all four photopigments, changes shape triggering the enzymatic activity of opsin. This leads to a activation of tranducin (the G protein contained in the rods and cones), which in turn depolarizes phosphodiesterase. This intracellular enzyme decreases the concentration of cyclic GMP (cGMP) which brings about the closure of the Na^+ channels[16]. Hence the potential across the membrane of the photoreceptor hyperpolarizes all the way to the synaptic terminal. The potential change leads to the closure of the Ca^{2+} channels

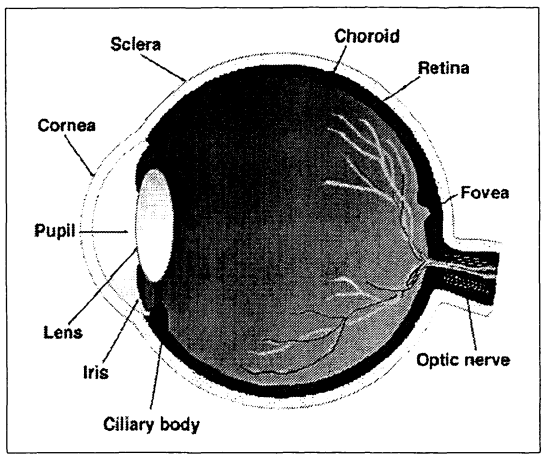

Figure 1: An overview of the eye. All borrowed figures courtesy of[8].

and a reduction in the glutamate neuro-transmitter release from the synaptic terminal. The amount of the hyperpolarization response and the reduction in the transmitter release depend on the intensity of the light photon. This leads to depolarization of the bipolar cells which exhibit graded potentials. The action potentials in the ganglion cells (the neurons between the bipolar cells and the optic nevers) propagates the visual signals to the brain[16]. See Fig. 1 for spatial organization of major components of the eye.

1.2 The Retina and Photoreceptors

The retina, literally an extension of the brain, is a crucial in the process of vision. The retina is a circular disk about 42mm in diameter found in the rear of the eye and is composed of three layers of nerve cell bodies and two layers of synapses (gaps between neurons)[8]. The three nerve cell layers include the outer nuclear layer, the inner nuclear layer, and the ganglion cell layer. The outer plexiform layer (OPL) and inner plexiform layer (IPL) bridge the gaps between these three cell layers[8].

The retina is not a homogeneous structure, but is instead characterized by diverse regions such as the fovea and optic disk which have different densities and spatial distributions of photoreceptors. The blood vessel free fovea, located directly in the back of the eye is the region with the highest

concentration of cones. In its center, the foveal pit, the cones reach their maximum density. In this rod free region, cones are ordered in a tight hexagonal arrangement[8]. The density of rods increases radially away from the fovea. The optic disk surrounds the attachment point of the optic nerve in the retina. The major blood vessels of the eye radiate outward non-uniformly from the optic nerve. Due to the bundling of nerve cells and blood vessels *no* photoreceptors are to be found in the optic disc[8]. See Fig 1.2 for rod and cone distribution in the retina.

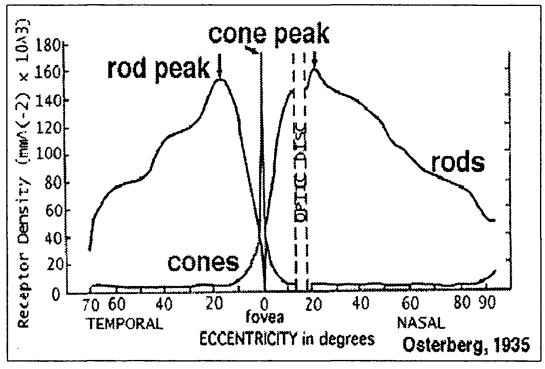

Figure 2: Rod and cone distribution[8]

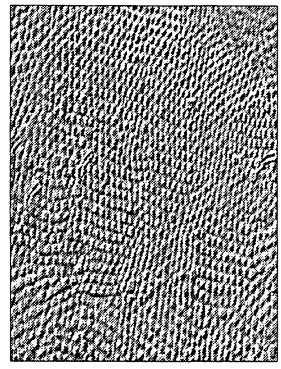

Cone packing in fovea[8]

Photoreceptors are in constant need of nutrient supply. They undergo continuous cellular renewal processes which depend on numerous biological factors. Following a circadian rhythm, rods and cones form and shed segment discs which are phagocytosed by the pigment epithelium, and through this process they regenerate completely about every 12 days, but this process can take up to 3 weeks[13]. Shedding requires numerous amino acids (precursors of opsin) and a great deal of intracellular energy all precursors of which must be delivered in the blood supply. In addition to the aforementioned factors, the blood supplied by the choroid contains other nutrients vital to photoreceptor survival. Synthesis of neurotransmitters such as glutamate, gamma aminobutyric acid, glycine, dopamine, acetylcholine, serotonin, and melatonin are crucial for rod and cone survival. Numerous neuropeptides are also required for proper neural function[8]. The trophic pool supplied by blood from the choroid is *vital* for photoreceptor survival.

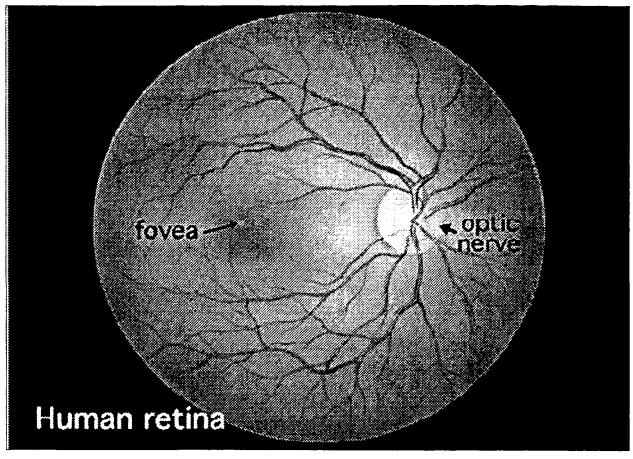

Figure 3: Overview of the normal retina[8]

1.3 Rod and Cone Morphology

The outer nuclear layer of the retina contains the cell bodies of the four types of photoreceptors–the rod and three types of cones (red, blue, and green) which each optimally receive light of different wavelengths due to differing photopigments[8]. Cones are larger structures and number approximately 6 million in the eye[19]. They "are conical cells which have their cell bodies located under the outer limiting membrane and their inner segments protrude into the subretinal space towards the pigment epithelium"[8]. Rods are much more numerous than cones, numbering about 120 million[19]. The rod cells are narrow, cylindrically shaped cells with their "inner and outer segments filling the area between the larger cones in the subretinal space and stretching to the pigment epithelium cells"[8].

Each photoreceptor can be subdivided into two components: a large opsin protein and a smaller retinene (a.k.a. retinal) molecule. Retinal is a derivative of vitamin A and is attached to the opsin. Retinal is the same in rods and cones, but the opsin protein differs in all four photopigments (actually called rhodopsin in rods)[13]. The fact that all opsins differ is crucial, as small genetic defects may only affect one type of photoreceptor as in some degenerative diseases (e.g. Retinitis pigmentosa).

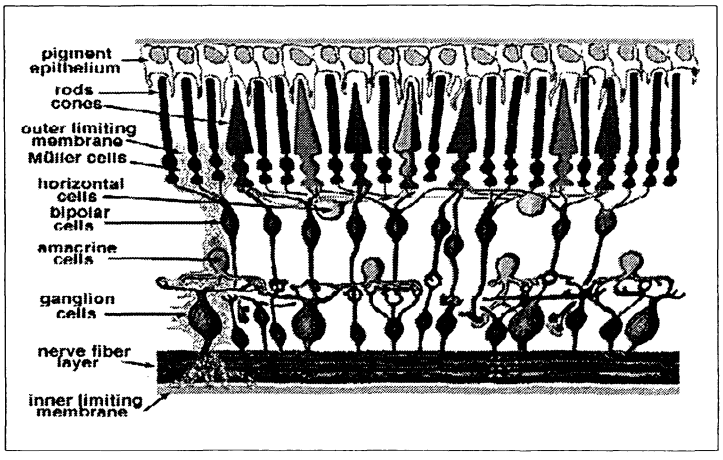

Figure 4: Rod and cone overview[8]

1.4 Rod and cone function

Difference in form translates into different functions in rods and cones. The vision pathway of the rods is highly convergent: between 15 and 30 rods synapse with a single rod bipolar cell in the outer plexiform layer. Having numerous rods synapse onto one bipolar cell aids in vision under low light conditions[8]. Rods synapse on only one type of bipolar cell, whereas the cones synapse on several different types which in turn synapse directly with ganglion cells. The synapsing rod bipolar cells, however, utilize intermediate amacrine cells. The rods achieve maximal density in a ring about 18^o from the fovea and this high rod density in the outer retina aids in peripheral vision. The high density of cones in the central fovea (a 6mm wide disk) and lack of horizontal cells (i.e. vertical transmission pathways) is responsible for acute central vision[13].

1.5 Interactions via horizontal cells and gap junctions

The inner nuclear layer of the retina contains the cell bodies of bipolar, horizontal, and amacrine cells. The horizontal cells have been implicated in direct photoreceptor interactions[8]. "Horizontal cells are characterized by large-surface-area gap junctions between dendrites of like type neighboring cells. These junctions allow lateral flow of electrical signals within syncitial

network of cells"[8]. Gap junctions connect phororeceptors of the same type as well as differing types. Horizontal cells send visual information back to cones through feedback loops, but there is currently no data supporting feedback back onto rods[8]. The gap junctional channels synchronize and regulate many intercellular activities in the retina and throughout the body[15].

Amacrine cells form intercellular pathways in the inner retina, and interplexiform cells form pathways from inner to outer retina. Both of these cell types have an effect of modulating signal flow between photoreceptors. Amacrine cells "integrate, modulate and interpose a temporal domain to the visual message presented to the ganglion cell"[8]. The output of rod bipolar cells goes to small AII amacrine cells whose output is onto the terminal end of cone bipolar cells. "Thus there are extra elements in the rod pathway such that the flow of information is rod $\rightarrow$ rod bipolar cell $\rightarrow$ AII amacrine cell $\rightarrow$ cone bipolar cell $\rightarrow$ ganglion cell"[13]. The interplexiform cells carry information in the direction opposite of bipolar cells; they direct information from inner to outer retina and have also been shown to modulate the information pathway[13]. The amacrine cells and interplexiform cells represent an interaction between information flow of rods and cones. It is likely that this interaction in information also represents, to a lesser degree, interaction between rods and cones.

1.6 Retinal Degeneration; Retinitis Pigmentosa

A gradual decrease in the number of rods and cones occurs over time even in healthy individuals. Extrapolating from a linear fit given in Oyster, we find about 34,000 rods are lost per year and about 57 cones are lost per year in the area surrounding the fovea. Given there are about 34,000 cones and 7,000,000 rods in this defined area, we can estimate the natural death rate of rods and cones in the whole eye to be about 600,000 rods per year and 10,060 cones per year[13].

This natural degradation of rods and cones, while affecting the quality of vision over a lifetime, is trivial compared to the devastating effects of several degenerative diseases. Millions of people suffer from accelerated retinal degeneration often leading to total blindness. Diseases such as Retinitis pigmentosa (RP), late-onset retinal degeneration (L-ORD), and age related

macular degeneration (AMD) have all been shown to usually affect rods first and to later extend to cones, resulting in total blindness[5]. Among these, RP is the primary cause of inherited blindness in the developed world, affecting 50,000-100,000 Americans alone[12][17].

Retinitis pigmentosa is a diverse group of inherited diseases typically characterized by initial loss of nearly all rods followed shortly thereafter by a slower loss of cones[10]. This progressive retinal degeneration manifests in an early loss of peripheral and night vision, and later by color blindness and finally loss of central vision[15]. The secondary loss of cones may progress over many decades, or sometimes much shorter periods. Different types of RP progress at different rates, but the rate is usually similar in family members[11].

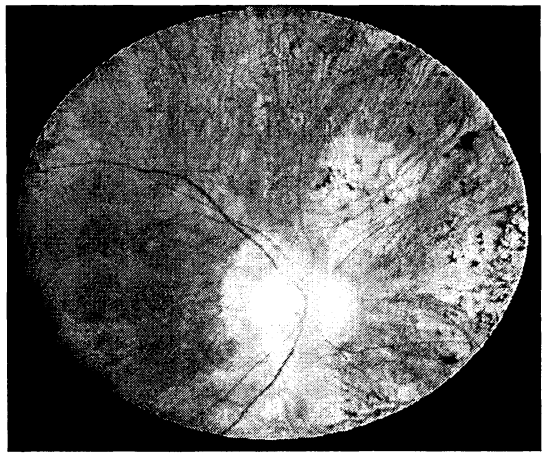

Figure 5: A retina affected by Retinitis pigmentosa: note the black pigment in the periphery and the thinned blood vessels at the optic nerve head.[8]

Mutations in more than 100 genes coding for proteins in the phototransduction cascade have been linked to RP[2]. "RP is inherited as an autosomal dominant disease in 43% of cases, autosomal recessive in 20%, and X-linked in 8%"[2]. The loss of cones comes somewhat unexpectedly as the mutations usually affect only the function of the rods and their phototransduction cascade.

1.7 Possible Causes for Secondary Cone Death in RP

There are two main hypotheses for the secondary wave of cone death in RP. Interactions–both intercellular and extracellular–are hypothesized to play a key role in transmission of toxic factors and trophic factors.

One explanation is that dying rods release toxic substances into the extracellular space which spur cone apoptosis (death). Glutamate and products of apoptosis are usually cited as candidates for the toxic substance. If the toxicity hypothesis is true, normal rods near defective rods would be expected to die at a faster rate than those far away simply by diffusion principles[15]. A study on mice by Huang et al. found uniform rod degeneration rates throughout normal and defective rod patches, thus contradicting the extracellular toxicity hypothesis[6]. Further, Kedzierski et al. (1998) found uniform degeneration in a mosaic pattern of transgene expression, also contradicting the toxicity hypothesis[15].

The second explanation is the existence of an extracellular trophic pool which rods and cones draw from and give to for survival. The crux of the trophic factor hypotheses is the assumption that beneficial factors necessary for cone survival are emitted by the rods, and the death of the cones results from deprivation of these factors following rod death. In support of the trophic factor hypothesis, several studies have shown that injection of specific factors can delay the wave of cone death[15].

A possible variation on the two previously mentioned hypotheses involves intercellular (direct cell to cell)–rather than extracellular–pathways. The toxic factors released from dying rods or trophic factors released from healthy rods could flow directly between cells. Harris Ripps advocates this "bystander effect", an effect mediated by direct cell-cell gap junctions. Ripps cites the toxicity factor as the more likely of the two hypotheses in this case, citing the study by Lin et al. (1998) as experimental support. Lin et al. showed that "dying glial cells undergoing apoptosis send death signals to their healthy neighbors via gap-junctional channels", and it is thus equally likely rods could do the same to cones[15].

If the intercellular toxicity hypothesis is true, the lack of horizontal cells in the center of the fovea should result in a slower degeneration of centrally located cones. Ripps points out, this does in fact occur[15]. The cones in the fovea, wired primarily in a one to one vertical arrangement necessary for acquisition of fine detail, are some of the last to be affected in the wave of cone death. Ripps further points out that while rods have been known to affect membrane potentials of cones, it has not been shown that cones regulate the rod membrane potentials. If this membrane polarization is beneficial to the photoreceptors, it could account for the lack of secondary rod cell death in degenerative diseases which primarily affect cones and the secondary wave of cone death in diseases like RP[15].

Further experimental study is needed to determine the source and method of propogation for the trophic or toxic factor responsible for the secondary wave of cone death. A better understanding will result in more efficacious treatments for retinal degenerations. Currently rod transplantation, intravitreal injection of survival factors, and oral supplementation of vitamin A are several treatments in RP[15].

2 The Disease Model

With a better understand of the biology of the eye disclosed, we now create a mathematical model. In our model we assume that the eyes are identical and hence consider only one eye. We postulate that cones and the rods interact directly with each other through intracellular connections involving the gap junctions between horizontal cells and indirectly through the trophic pool. We model the flow of nutrients between the photoreceptors as an epidemiological process. We imagine that both the normal rods (R_n) and the cones (C) take more nutrients from the trophic pool (T) than they contribute, and that they convert these trophic factors to new cells at some ratio. We consider mutations on the rhodopsin molecule (which is contained only in the rods) and assume that the mutated rods (R_m) communicate indirectly with other healthy rods and cones through the trophic pool. Once the rhodopsin molecule is mutated, it transforms a normal rod into mutated rod. The diseased (or mutated) rod lives only temporarily, but through its short residence time is still capable of affecting other rods and cones. We

illustrate the positive directional nutrient flow from the trophic pool to all photoreceptors. We consider the trophic pool to supplied with nutrients at a constant influx rate which is dependent on the size of the pool. The constant recruitment rate into the trophic implies that if withdrawal rate exceeds influx rate the pool will empty. Conversely, in the absence of rods the pool will grow exponentially. See flow diagram (Figure 6), in which all parameters are positive.

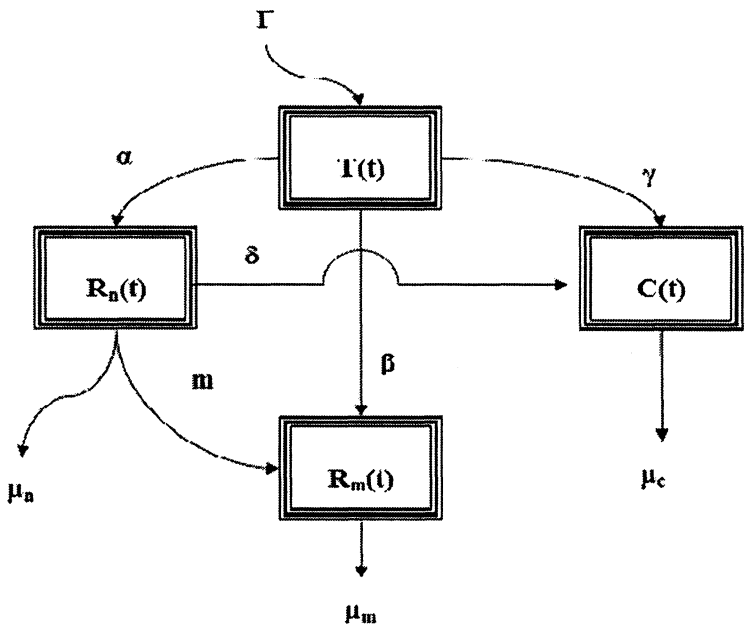

Figure 6: The disease model

We formulate the system of differential equations from the flowchart and our assumptions.

$$\begin{aligned}
\dot{R_n}(t) &= R_n(t)(aT(t) - \mu_n - m) \\
\dot{R_m}(t) &= R_m(t)(bT(t) - \mu_m) + R_n(t)m \\
\dot{C}(t) &= C(t)(cT(t) - \mu_c + dR_n(t)) \\
\dot{T}(t) &= T(t)(\Gamma - \alpha R_n(t) - \beta R_m(t) - \gamma C(t)
\end{aligned} \tag{1}$$

Here α and γ represent the exchange rate of nutrients from the trophic pool to the healthy rods and cones, respectively. Once the rods are invaded by the disease they mutate at a rate m. The per cell transfer rate of nutrients from the trophic pool to the mutated rods is defined as β. The per cell rate at which nutrients and signals move between the healthy rods and the cones through the horizontal cells is given by δ. The $\dot{R_n}$, $\dot{R_m}$, and $\dot{C}$ equations all have a conversion factor associated with them. This conversion factor arises from an assumption that one unit of trophic factor does not result in exactly one new photoreceptor. Hence we have $a = \alpha q_1$, where q_1 is the conversion accounting for each unit of trophic factor that gets converted into rod, likewise for the other systems. The rods help the cones (without hurting themselves) at a rate δ and the cones convert this to new cones at a factor q_4. R_n, R_m, and C leave the system at natural death rates μ_n, μ_m, and μ_c respectively. These assumptions are summarized in table 7.

2.1 Full Model With Delay

To account for the delay in the secondary degeneration wave of photoreceptors we have considered a fixed time delay (τ) on the direct communication media between the cones and the rods. This changes the set of equations only slightly:

$$\begin{aligned}
\dot{R_n}(t) &= R_n(t)(aT(t) - \mu_n - m) \\
\dot{R_m}(t) &= R_m(t)(bT(t) - \mu_m) + R_n(t)m \\
\dot{C}(t) &= C(t)(cT(t) - \mu_c + dR_n(t - \tau)) \\
\dot{T}(t) &= T(t)(\Gamma - \alpha R_n(t) - \beta R_m(t) - \gamma C(t))
\end{aligned} \tag{2}$$

Variable	Description	Units
Γ	Total inflow rate into the trophic pool	1/t
α	Constant per cell rate at which R_n withdraws T	$1/R_n$t
β	Constant per cell rate at which R_m withdraws T	$1/R_m$t
γ	Constant per cell rate at which C withdraws T	1/Ct
δ	Constant per cell rate at which R_n helps C	1/Ct
q_1	Per cell conversion factor	R_n/T
q_2	Per cell conversion factor	R_m/T
q_3	Per cell conversion factor	C/T
q_4	Per cell conversion factor	C/R_n
μ_n	Per cell death rate of R_n	1/t
μ_m	Per cell death rate of R_m	1/t
μ_c	Per cell death rate of C	1/t
m	Per cell mutation rate of R_n	1/t
a	αq_1	1/Tt
b	βq_2	1/Tt
c	γq_3	1/Tt
d	δq_4	$1/R_n$t

Figure 7: Value of parameters for our model

This framework allows the investigation of the effect of mutants on cones and rods via their effect on the flow of nutrients and signal information. We begin by investigating the relationship between rods and cones in a mutation free individual.

3 The Model Without Disease

We can illustrate the dynamics of the interactions between the rods and the cones for an individual without RP (i.e., a healthy person) by letting $R_m = m = \mu_m = b = 0$. Imposing such conditions on the original system, equations (1), reduces the system to 3 dimensions.

3.1 The Disease Free Model Without Delay

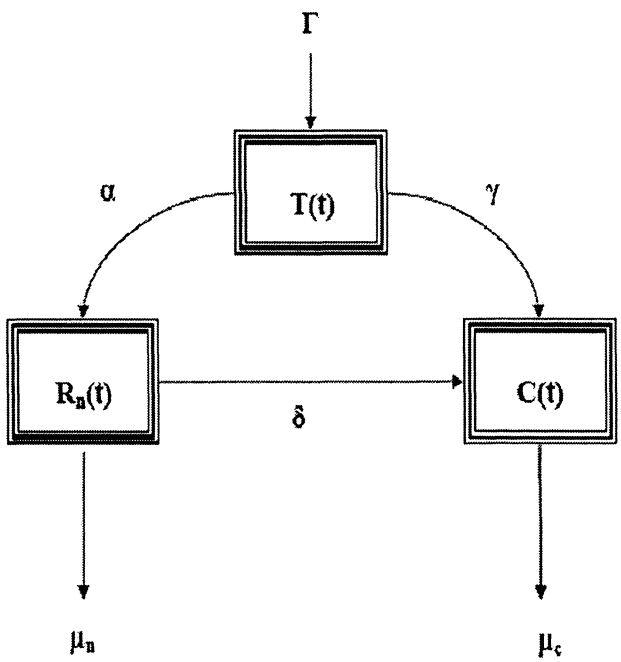

Figure 8: The disease free model.

The governing dynamics of an eye without RP are given by

$$\begin{aligned} \dot{R}_n(t) &= R_n(t)(aT(t) - \mu_n) \\ \dot{C}(t) &= C(t)(cT(t) - \mu_c + dR_n(t)) \\ \dot{T}(t) &= T(t)(\Gamma - \alpha R_n(t) - \gamma C(t)) \end{aligned} \tag{3}$$

Here the parameters have the same meaning as in equations (1). The mechanism between the trophic pool (T), the normal rods (R_n), and the cones (C) is presented in the flow diagram Figure 8.
We begin by studying the long term behavior of the system given by equations (3). The logical first step is to compute the steady state solutions. The equilibria are obtained by setting the right hand of (3) to zero and solving for the independent variables. Following these steps we obtain four equilibria $(E_i, i = 1, 2, 3, 4)$ which we will denote in the form (R_n^*, C^*, T^*).

$$\begin{aligned} E_1 &: \quad (0, 0, 0) \\ E_2 &: \quad \left(0, \tfrac{\Gamma}{\gamma}, \tfrac{\mu_c}{c}\right) \\ E_3 &: \quad \left(\tfrac{\Gamma}{\alpha}, 0, \tfrac{\mu_n}{a}\right) \\ E_4 &: \quad \left(\tfrac{-c\mu_n + a\mu_c}{ad}, \tfrac{\Gamma ad + \alpha c\mu_n - \alpha a\mu_c}{\gamma ad}, \tfrac{\mu_n}{a}\right) \end{aligned} \tag{4}$$

Having solved for the equilibria of the system, we then analyze the local stabily of the equilibria by linearization. In other words, we determine the local stability by investigating the eigenvalues of the linearized system. Hence, the jacobian for the system is:

$$J = \begin{pmatrix} \Gamma - \alpha R_n - \gamma C & -T\alpha & -T\gamma \\ aR_n & aT - \mu_n & 0 \\ Cc & Cd & cT - \mu_c + dR_n \end{pmatrix}.$$

The characteristic equation for the equilibrium E_i is given by

$$\mid J_E - \lambda I_3 \mid = 0.$$

Applying this procedure to all four equilibria yields the eigenvalues E_i:

$$\begin{aligned}
\lambda(E_1): &\quad (\Gamma, -\mu_n, -\mu_c) \\
\lambda(E_2): &\quad \left(\tfrac{-c\mu_n + a\mu_c}{c}, \sqrt{-\Gamma\mu_c}, -\sqrt{-\Gamma\mu_c}\right) \\
\lambda(E_3): &\quad \left(\tfrac{\Gamma da + \alpha c\mu_n - \alpha\mu_c a}{a\alpha}, \sqrt{-\Gamma\mu_n}, -\sqrt{-\Gamma\mu_n}\right).
\end{aligned} \tag{5}$$

The eigenvalues for the E_4 are too lengthy (pages long) to show here, but all eigenvalues have nonzero have real part. The instability associated to E_4, however, is not difficult to show. The stability of the steady state solution is determined by the real part of the eigenvalues. An equilibrium is locally asymptotically stable if all eigenvalues have negative real part[9],[14]. If $\Re($ λ $)= 0$ for any λ then the point is non–hyperbolic and the local analysis of the system cannot be determined from linearization. In such cases the original nonlinear system is not topologically equivalent to the linear system in a small neighborhood about the equilibria. In other words, under nonhyperbolic fixed points there is no diffeomorphism between the nonlinear system and the linear system in a small neighborhood about the equilibrium. Hence higher order terms can not be ignored in analyzing the local behavior of the system[9],[14].

From our eigenvalues it is clear that E_1 and E_4 are hyperbolic fixed points. It is also clear that E_2 and E_3 are nonhyperbolic fixed points. Linear analysis of E_1 shows that the origin always exists, and since $\Gamma > 0$ it is always unstable. The "healthy human" equilibrium point (E_4) exists biologically when

$$a \in \left(\frac{\mu_n c}{\mu_c}, \frac{\alpha c\mu_n}{\alpha\mu_c - \Gamma d}\right)$$

provided we make the assumption $\Gamma d - \alpha\mu_c < 0$.

In determining stability of E_4, we use the Routh-Hurwitz criteria on the characteristic polynomial:

$$\begin{aligned}
p(\lambda) = \lambda^3 &- \frac{\alpha ac\mu_n^2 - acd\mu_n\Gamma - \alpha a^2\mu_n\mu_c - \alpha c^2\mu_n^2 + \alpha ac\mu_n\mu_c}{a^2 d}\lambda \\
&- \frac{-2\alpha ac\mu_c\mu_n^2 + acd\Gamma\mu_n^2 + \alpha c^2\mu_n^3 - a^2 d\mu_c\mu_n\Gamma + \alpha a^2\mu_n\mu_c^2}{a^2 d}
\end{aligned} \tag{6}$$

For stability, the Routh-Hurwitz criteria requires a characteristic polynomial of the form $\lambda^3 + a_1\lambda^2 + a_2\lambda + a_3$ to have $a_1 > 0$. Clearly that is not the case with E_4 since the cooefficient on the λ^2 term is 0. The "healthy human" equilibria is always unstable[3],[9],[14].

3.1.1 Dynamic Behavior of Nonhyperbolic Fixed Points

The model undergoes extremely interesting dynamic behavior around the nonhyperbolic fixed points E_2 (which lives in the invariant C-T plane) and E_3 (which lives in the invariant R_n-T plane). Interpretation of the solutions close to E_2 and E_3 for initial conditions in these invariant planes provides valuable biological insight. Setting $R_n = 0$ we see the set of equations reduces to the 2-dimensional system,

$$\begin{aligned} \dot{C} &= C(t)(cT(t) - \mu_c), \\ \dot{T} &= T(t)(\Gamma - \gamma C(t)). \end{aligned} \tag{7}$$

Similarly, setting $C = 0$ reduces our system to 2-dimensions and, the mathematical expressions become

$$\begin{aligned} \dot{R}_n &= R_n(t)(aT(t) - \mu_n), \\ \dot{T} &= T(t)(\Gamma - \alpha R_n(t)). \end{aligned} \tag{8}$$

This behavior implies that once an individual loses all rods or cones (and enters an invariant plane), they can never regain them. If a person is born with no rods or cones, they will also never gain them, as spontaneous generation of photoreceptors does not occur[15]. This fact is accurately reflected in this model.

Furthermore, dynamics about each of the equilibrium points in their respective planes is intriguing. The eigenvalues of E_2 are $\sqrt{-\Gamma\mu_c}$ and $-\sqrt{-\Gamma\mu_c}$ which, given the assumptions on the parameters, are both purely imaginary. The eigenvalues of E_3 are $\sqrt{-\Gamma\mu_n}$ and $-\sqrt{-\Gamma\mu_n}$ which also have no real part for $\Gamma > \mu_n > 0$. Thus we have either a family of centers or weak focus around each of these points in their respective planes[14], [9]. The system in the R_n-T plane given in 44, can be written in terms of x and y as

$$\begin{aligned} \dot{T} &= by + p(x, y) \\ \dot{y} &= cx + q(x, y) \end{aligned}$$

where $p(x,y) = -\alpha TR_n$ and $q(x,y) = aTR_n$.
Following a thereom in Perko, wherein we characterize the stability behavior of the nonhyperbolic equilibriam through the Liapunov number[14]:

$$\begin{aligned}\dot{x} =& ax + by + p(x,y)\\ \dot{y} =& cx + dy + q(x,y)\end{aligned}$$

Note that in our case $a = d = 0$ and $R_n = y, T = x, \dot{R}_n = \dot{y}, \dot{T} = \dot{x}$.

$$\begin{aligned}\dot{T} =& by + p(x,y)\\ \dot{y} =& cx + q(x,y)\end{aligned} \tag{9}$$

we substitute $R_n = y, T = x, \dot{R}_n = \dot{x}, \dot{T} = \dot{y}$. As we have a nonhyperbolic equilibrium (i.e $\Re(\lambda) = 0$ for at least one of the eigenvalues), we must look at higher order terms. In our case we have

$$p(T, R_n) = \sum_{i+j\geq 2} d_{i,j} T^i R_n^j = d_{20}T^2 + d_{11}TR_n + d_{02}R_n^2 = aTR,$$

which shows

$$d_{11}TR_n = aTR_n$$

Further,

$$q(T, R_n) = \sum_{i+j\geq 2} b_{i,j} T^i R_n^j = b_{20}T^2 + b_{11}TR_n + b_{02}R_n^2 = -\alpha TR$$

which results in

$$b_{11}TR_n = -\alpha TR_n$$

We don't consider the other orders because they do not exist in our model.
The Liapanov number σ is given by the equation

$$\sigma = \frac{3\pi}{2b}\{3[(a_{30} + b_{03}) + (a_{12} + b_{21})] - \frac{2}{b}[(a_{20}b_{20} - a_{02}b_{02}) - a_{11}(a_{02} + a_{20}) + b_{11}(b_{02} + b_{20})]\} \tag{10}$$

and in our case $a_{ij} = d_{ij}$. If we substitute we find $\sigma = 0$. If $\mu = \sigma = 0$, then the rod free equilibrium is a weak focus of multiplicity $m > 1$, and the cone free equilibrium follows by symmetry[14].

3.1.2 Level curves

We have characterized the rod free and cone free hyperbolic fixed points as weak foci of mulitplicity > 1, and now we seek the associated level curves.

Recall the equations in the R_n-T plane

$$\begin{aligned} \dot{T} =& \Gamma T - \alpha T R_n \\ \dot{R_n} =& -R_n \mu_n + aTR_n. \end{aligned} \tag{11}$$

In considering the cone free equilibrium in its respective invariant plane, we now have a predator-prey system where T is the prey and R_n is the predator. We recall the equation in the R_n-T invariant plane to compute the level curves.

$$\frac{dR_n}{dT} = \frac{-\mu_n R_n + aTR_n}{\Gamma T - \alpha T R_n} \tag{12}$$

To solve this problem we use separation of variables.

$$\frac{dR_n}{dT} = \frac{TR_n\left(\frac{-\mu_n}{T} + a\right)}{TR_n\left(\frac{\Gamma}{R_n} - \alpha\right)} \tag{13}$$

We separate variables and integrate

$$\begin{aligned} \int \left(\frac{\Gamma}{R_n} - \alpha\right) dR &= \int \left(\frac{-\mu_n}{T} + a\right) dT \\ \Gamma \ln R_n - \alpha R_n &= -\mu_n \ln T + aT + K_0 \\ f(T, R_n) &= \ln T^{(\mu_n)} R_n^{(\Gamma)} - (aT + \alpha R_n + K_0). \end{aligned} \tag{14}$$

The function $f(T, R_n)$ are the level curves defining the motion of the system. For each different constant K_0 there exists a different curve projected

onto the (T, R_n) plane.

Exponentiating yields

$$(R_n)^{(\Gamma)}T^{(\mu_n)} = e^{(aT+\alpha R_n+K_0)} = e^{(aT)}e^{(\alpha R_n)}K. \tag{15}$$

Hence $R_n^{(\Gamma)}e^{(-\alpha R_n)} = \frac{Ke^{(aT)}}{T^{(\mu_n)}}$, where K is constant. The steady state is in the point$(\frac{\Gamma}{a}, \frac{\mu_n}{\alpha})$. If we compute the nullclines that implies, we found the trivial solution

$$R^* = 0 \text{ and } T^* = 0$$

and the non-trivial solution

$$R^* = \frac{\Gamma}{\alpha} \text{ and } T^* = \frac{\mu_n}{a}$$

If we use the non trivial solution and substitute $T^* = \frac{\mu_n}{a}$ in the equation (15) we get $R_n^{(\Gamma)}e^{(-\alpha R_n)} = \frac{Ke^{(\Gamma a)}}{\Gamma}$ and this solution is constant. This proves that E_2 and similarly E_3 are centers. If we graph the function $f(R_n) = R_n e^{-\alpha R_n}$ and $f(y) = \frac{Ke^{\Gamma a}}{\Gamma}$ we see

In the graph of Figure 9 we can see that $f(R_n)$ and $f(y)$ have at most 2 solutions for any given constant. If we trace a line in $T = \frac{\mu_n}{a}$ we see that this line intersects the graphs 2 times; therefore the trajectory can't be a spiral[9],[14]. Refer to Figures 10 and 11 for graphical representation of the level curves.

We show that in the cone free equilibrium point E_2 we have a weak focus or multiple focus. We see this situation graphically in Figure 10 and Figure 11, which shows numerically that we have "circles" but not limit cycles. These curves are modeled by the function

$$f(T, R_n) = \ln TR_n - (aT + \alpha R_n + K)$$

where K is a constant. We obtain the same results with $R_n = 0$ and $C \neq 0$. When this happens we don't know the stability of the system. Biologically that means that the rods or cones and the trophic factor change but satisfy an equation that remains constant. The systems can have neutrally stable cycles, but not limit cycle trajectories[4].

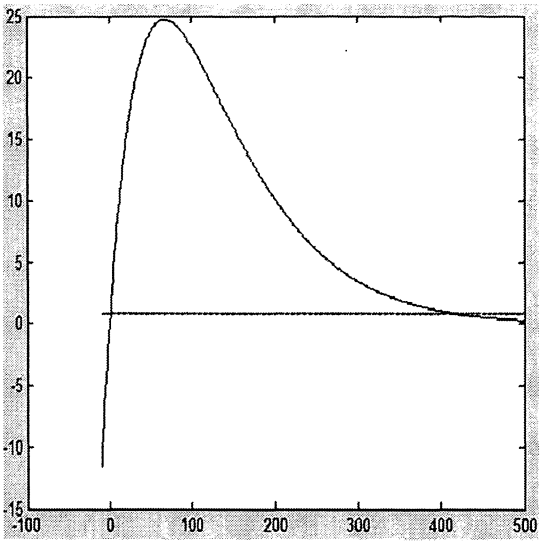

Figure 9: Graphical proof of the equation is no spiral

3.1.3 Rods, Cones, and Trophic Factor as a Two Predator-Single Prey System

"The fact that predator-prey systems have a tendency to oscillate has been observed for well over a century"[4]. The oscillations observed in our model force us to ask: could rods and cones be preying on the trophic factor? A standard two predator-prey system with x as the prey and y_1 and y_2 as the predators are governed by the following equations[1]:

$$\begin{aligned} \dot{x} =& ax - b_1 x y_1 - b_2 x y_2 \\ \dot{y_1} =& -c_1 y_1 + d_1 x y_1 \\ \dot{y_2} =& -c_2 y_2 + d_2 x y_2 \end{aligned} \tag{16}$$

This set of equations corresponds nearly exactly with ours, if we let $x = T, y1 = R_n, y2 = C$. The exception is that we have an extra dR_n term in our $\dot{C}$ equation. In our case, the rod predator helps the cone predator, whereas in the above equation the predators have no interaction. Let us temporarily neglect this extra factor in our $\dot{C}$ equation (we are neglecting direct cell-cell communication), thus giving us a standard predator-prey model. We then

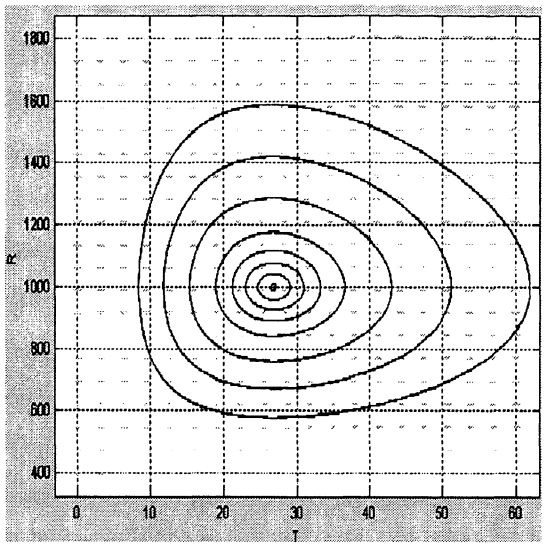

Figure 10: The rods and trophic factor's weak foci

have the system of equations:

$$\begin{aligned} \dot{T} &= T(t)(\Gamma - \alpha R_n(t) - \gamma C(t)) \\ \dot{R_n} &= R_n(t)(aT(t) - \mu_n) \\ \dot{C} &= C(t)(cT(t) - \mu_c) \end{aligned} \tag{17}$$

In this case it has been shown that "one of the predator populations always drives out the other".[4] This is in fact the case in our system. The equilibrium points of this system are given by (R_n,C,T):

$$\begin{aligned} E_1 &: \quad (0,0,0), \\ E_2 &: \quad \left(0, \tfrac{\Gamma}{\gamma}, \tfrac{\mu_c}{c}\right), \\ E_3 &: \quad \left(\tfrac{\Gamma}{\alpha}, 0, \tfrac{\mu_n}{a}\right). \end{aligned} \tag{18}$$

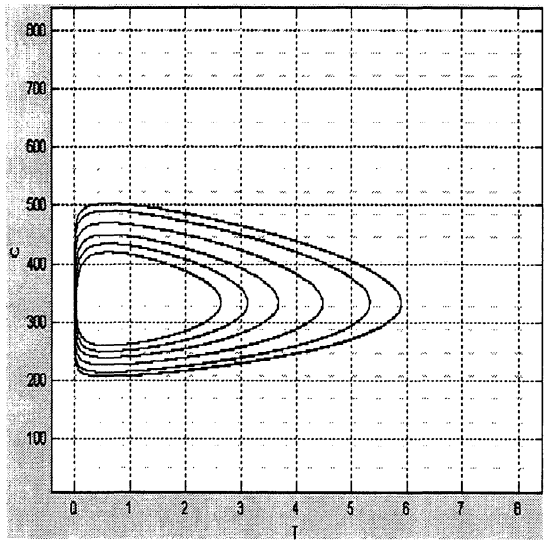

Figure 11: The cones and trophic factor's weak foci

The corresponding eigenvalues:

$$\begin{aligned} \lambda(E_1): &\quad (\Gamma, -\mu_n, -\mu_c) \\ \lambda(E_2): &\quad \left(\tfrac{-c\mu_n + a\mu_c}{c}, \sqrt{-\Gamma\mu_c}, -\sqrt{-\Gamma\mu_c}\right) \\ \lambda(E_3): &\quad \left(\tfrac{c\mu_n - a\mu_c}{c}, \sqrt{-\Gamma\mu_n}, -\sqrt{-\Gamma\mu_n}\right). \end{aligned} \tag{19}$$

It is clear that one of E_2 or E_3 is unstable at all times, thus showing that rods and cones can not coexist. Biologically, this means that if there is no commensalistic factor between the rods and cones in our model, only one of the two photoreceptors will survive as $t \to \infty$. The possibility of coexistence is dependent on the dR_n term in the $\dot{C}$ equation in this case. This strongly suggests the existence of the direct interaction term.

3.1.4 Complete Three Trophic Level System

Although there is strong evidence that the cones are helped by the presence of the rods, there does not seem to be evidence which suggests that the rods are even somewhat hurt by the cones. One explanation of why this effect may not have been observed could be that because the rods so greatly outnumber

the cones the harmful effect that the cones have on the rods is minimal. Mathematically, however, we could model this interaction by including an additional term in the equation for $C(t)$. The full model with delay is then given by

$$\frac{dR_n}{dt} = R_n(t)\,(a\,\mathrm{T}(t) - \mu_n - e\,\mathrm{C}(t)) \tag{20}$$

$$\frac{d\mathrm{C}}{dt} = \mathrm{C}(t)\,(c\,\mathrm{T}(t) - \mu_c + d\,R_n(t-\tau)) \tag{21}$$

$$\frac{d\mathrm{T}}{dt} = \mathrm{T}(t)\,\Gamma - (\alpha\,R_n(t) + \gamma\,\mathrm{C}(t))\,\mathrm{T}(t) \tag{22}$$

When there is no delay in the model, the results are well-known.[1] In particular, the results state that all three variables we consider cannot coexist—one must die.

For the non-delay equations, the curve along which Hopf bifurcations may occur is given by

$$F_1(-\mu_c\,\alpha\,e + d\,\Gamma\,e + d\,\gamma\,\mu_n) = 0 \tag{23}$$

where

$$F_1 = (-a\,\mu_c\,\alpha + a\,d\,\Gamma + \mu_n\,c\,\alpha)\,(\Gamma\,c\,e - \gamma\,a\,\mu_c + \gamma\,\mu_n\,c) \tag{24}$$

Incorporating the time delay gives a new curve:

$$\tau = \frac{3\,F_2\,(-\alpha\,c\,e + \gamma\,d\,a)}{-F_1(2\,\gamma\,d\,a + \alpha\,c\,e)} \tag{25}$$

where

$$F_2 = (\gamma\,\alpha\,\mu_c\,a^2 + \gamma\,c\,\Gamma\,d\,a - \gamma\,a\,\alpha\,c\,\mu_n - \gamma\,a\,c\,\alpha\,\mu_c + \gamma\,\alpha\,c^2\,\mu_n - \alpha\,e\,c\,\Gamma\,a) \tag{26}$$

and we have assumed that the delay is small in order to obtain a closed form analytical expression. See the next section for a full derivation of the analogory results for the system where we assume the rods help the cones but are not hurt by them.

Numerical solutions of the delay equation again showed oscillatory behavior.

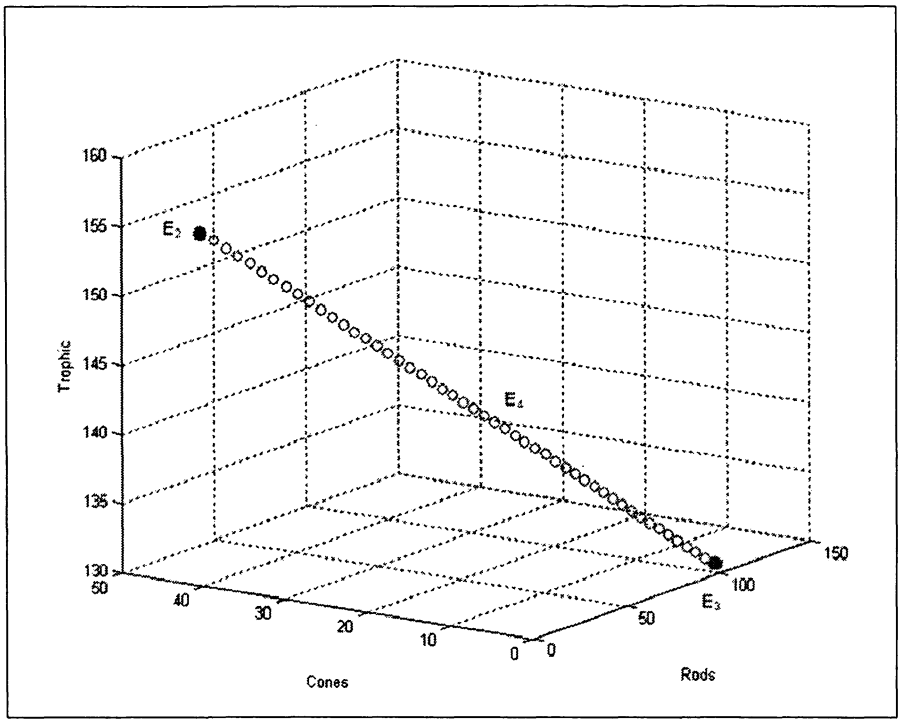

Figure 12: (a) $a = .0045, \tau = 0$ (b)$a = .0045, \tau = 1$

3.1.5 Fold-Hopf Bifurcation at the "healthy human" equilibrium ($\tau = 0$

Recall that the healthy human equilibrium E_4, which is always *unstable*, is *biologically relevant and unique* when the parameter a satisfies

$$a \in \left(\frac{\mu_n c}{\mu_c}, \frac{\alpha c \mu_n}{\alpha \mu_c - \Gamma d} \right) = (a^o, a^*)$$

The evolution of the "healthy human" E_4 across the biologically relevant region (i.e. the 1st Octant) is shown in Figure 12. Note that when $a = \frac{\mu_n c}{\mu_c} = a^o$, E_4 and E_2 coincide (they are the same point mathematically). Similiary, when $a = \frac{\alpha c \mu_n}{\alpha \mu_c - \Gamma d} = a^*$, E_4 and E_2 coincide.

Therefore, this makes these two a values prime candidates for bifurcation analysis, which we do now.

First, we explored the possibility that for certain parameter values there may exists a limit cycle (suggested by numerical solutions). The emergence and/or disappearance of these limit cycles would correspond to a Hopf bifurcation. In order to locate a Hopf bifurcation we look for eigenvalues of the form

$$\lambda = iw$$

where $w \in \mathbb{R}^+$. Making this substitution into $\mid A - \lambda I_3 \mid = 0$ gives

$$\lambda^3 + e\lambda + f = -iw^3 + iew + f$$

where e, $f \in \mathbb{R}$. This implies

$$iw(-w^2 + e) + f = 0$$
$$\text{or}$$
$$f = 0 \text{ and } w^2 = e$$

Recalling that $w \in \mathbb{R}^+$, it is clear $e > 0$. So for the Hopf bifurcation to occur, we have the conditions $e > 0$ and $f = 0$.
In the case of our system the parameters have the values

$$e = \frac{\mu_n(\Gamma acd + \alpha c^2\mu_n - \alpha ac\mu_c - \alpha ac\mu_n + \alpha a^2\mu_c)}{a^2 d}$$

$$f = \mu_n(c\mu_n - a\mu_c)(\alpha c\mu_n - \alpha a\mu_c + \Gamma ad)$$

We solve $f = 0$ for a which gives

$$a = \frac{c\mu_n}{\mu_c} = a^o \qquad \text{or} \qquad a = \frac{\alpha c\mu_n}{\alpha\mu_c - \Gamma d} = a^*$$

This shows that at both of these a values the eigenvalues are purely imaginary (a Hopf bifurcation), and suggests that we should expect oscillations for all values of a between these two critical Hopf values. Numerical solutions (see the following section) indeed verified this intuition and again suggested that the limit cycle which occurs between these two parameter values is stable.

Now, we investigate other possible bifurcations that may occure when $a = a^o$ or when $a = a^*$. In looking for bifurcations at $a = a^o$, we consider

the point E_2 for two reasons. Firstly, E_2 lies in the plane in which $R_n = 0$ (recall, we know quite a good deal about the behaviors of solutions confined in this plane). Secondly, recall that when $a = a^o$, E_2 and E_4 coincide. Here, we represent the eigenvalues for the point E_2:

$$(\lambda_1(E_2), \lambda_2(E_2), \lambda_3(E_2)) = \left(\frac{-c\mu_n + a\mu_c}{c}, \sqrt{-\Gamma\mu_c}, -\sqrt{-\Gamma\mu_c}\right)$$

Note that for all values of a, $\lambda_2(E_2)$ and $\lambda_3(E_2)$ are always purely imaginary. This suggests that solutions should spiral in the two eigendirections corresponding to these purely imaginary eigenvalues. However, $\lambda_1(E_2)$ is real and can be considered as function of a (assuming all other parameter values are held constant). Therefore, this analysis will focus only on $\lambda_1(E_2)$. Consider the follwing results, which were determined numerically.

$\lambda_1(E_2)|_{(a<a^0)} < 0 \quad \Rightarrow \quad$ The point E_2 in the invariant plane $R_n = 0$ is *attracting*
$\lambda_1(E_2)|_{(a>a^0)} > 0 \quad \Rightarrow \quad$ The point E_2 in the invariant plane $R_n = 0$ is *repelling*

Here, we showed numerically that for values of $a < a^o$, the plane appears to be attracting oscillating solutions. See Figure 15 for a numerical simulation. For values of $a > a^o$, the plane appears to be repelling oscillation solutions. Now, we consider the case where $a = a^o$, which leads to an interesting result.

$\lambda_1(E_2)|_{(a=a^0)} = 0 \Rightarrow$ The point E_2 in the invariant plane $R_n = 0$ is *neutral*

Here, if we examine all three eigenvalues for E_2 when $a = a^o$ and keeping in mind that at this value of a, $E_2 = E_4$, we see that

$$\lambda_1(E_4) = \lambda_2(E_2) = (0, i\sqrt{\Gamma\mu_c}, -i\sqrt{\Gamma\mu_c})$$

This form of these eigenvalues is special, and states that when $a = a^o$ (i.e. when the equilibria E_4 and E_2 are equal), a Fold-Hopf bifurcation occurs. Simply put, this means when $a = a^o$, the point E_2 in the plane R_n=0 changes from attracting to repelling *at the same time that a limit cycle is born.*

A similar analysis is done to investigate other possible bifurcations when the parameter $a = a^*$. Analagously, we chose to consider the equilibrium E_3 because the behavior of solutions confined to the plane in which $C = 0$, where E_3 lives, are well understood and because when the bifurcating parameter $a = a^*$, $E_3 = E_4$.

$$(\lambda_1(E_3), \lambda_2(E_3), \lambda_3(E_3)) = \left(\frac{\Gamma d a \alpha(c\mu_n - a\mu_c)}{a\alpha}, \sqrt{-\Gamma\mu_n}, -\sqrt{-\Gamma\mu_n}\right)$$

Like the previous case, for all values of a, $\lambda_2(E_3)$ and $\lambda_3(E_3)$ are always purely imaginary, which implies oscillating solutions. Once again like the previous case, we will be interested only in the behavior of $\lambda_1(E_3)$. Shown below are more results we were able to gain numerically (See Figure 19).

$\lambda_1(E_3)|_{(a<a^*)} > 0 \quad \Rightarrow$ The point E_3 in the invariant plane $C = 0$ is *repelling*
$\lambda_1(E_3)|_{(a>a^*)} < 0 \quad \Rightarrow$ The point E_3 in the invariant plane $C = 0$ is *attracting*

Here, we numerically showed that that when $a < a*$, the plane appears to be repelling oscillating solutions whereas when $a > a*$, the plane seems to be attracting them. Here, we also find interesting results when $a = a^*$.

$\lambda_1(E_3)|_{(a>a^*)} < 0 \Rightarrow$ The point E_3 in the invariant plane $C = 0$ is *attracting*
and
$\lambda_1(E_3) = \lambda_2(E_3) = (0, i\sqrt{\Gamma\mu_n}, -i\sqrt{\Gamma\mu_n})$

So, we again find another *Fold-Hopf bifurcation.* At the value $a = a^*$, the point E_3 in the plane $C = 0$ changes from repelling to attracting at the same time that we numerically see that *the limit cycle collapses and ceases to exist.*

3.2 The Model With Delay

The equations are modified slightly to include the delay term, τ:

$$\begin{aligned}
\dot{R_n} &= R_n(t)(aT(t) - \mu_n) \\
\dot{C} &= C(t)(cT(t) - \mu_c + dR_n(t-\tau)) \\
\dot{T} &= T(t)(\Gamma - \alpha R_n(t) - \gamma C(t))
\end{aligned} \tag{27}$$

The equilibria of the system with delay are identical to the equilibria in the system without delay, see equation 4. The stability of the equilibria may change depending on the delay τ. To determine the stability, we linearize by letting

$$R_n(t) = u_1(t) + \frac{-c\mu_n + \mu_c a}{da} \tag{28}$$

$$R_n(t-\tau) = u_1(t-\tau) + \frac{-c\mu_n + \mu_c a}{da}, \tag{29}$$

$$C(t) = u_2(t) + \frac{\Gamma da + \alpha c\mu_n - \alpha\mu_c a}{\gamma da} \tag{30}$$

$$T(t) = u_3(t) + \frac{\mu_n}{a} \tag{31}$$

be small perturbations about the in-phase mode. We substitute equations (28)-(31) into equations 3. Ignoring higher order terms, we obtain

$$\frac{du_1}{dt} = a\,u_3(t)\,u_1(t) - \frac{u_3(t)\,c\,\mu_n}{d} + \frac{a\,u_3(t)\,\mu_c}{d} \tag{32}$$

$$\begin{aligned}
\frac{du_2}{dt} &= u_2(t)\,c\,u_3(t) + u_2(t)\,d\,u_1(t-\tau) + \frac{\Gamma\,c\,u_3(t)}{\gamma} + \frac{\Gamma\,d\,u_1(t-\tau)}{\gamma} + \frac{\alpha\,c^2\,\mu_n\,u_3(t)}{\gamma\,d\,a} \\
&\quad + \frac{\alpha\,c\,\mu_n\,u_1(t-\tau)}{\gamma\,a} - \frac{\alpha\,\mu_c\,c\,u_3(t)}{\gamma\,d} - \frac{\alpha\,\mu_c\,u_1(t-\tau)}{\gamma}
\end{aligned} \tag{33}$$

$$\frac{du_3}{dt} = -\frac{(a\,u_3(t) + \mu_n)\,(\alpha\,u_1(t) + u_2(t)\,\gamma)}{a} \tag{34}$$

Since equations (32)-(34) give a system of linear homogeneous equations with constant coefficients, we seek solutions of the form

$$u_1 = (u_0)_1 \cdot e^{\lambda t},\quad \widetilde{u}_1 = (u_0)_1 \cdot e^{\lambda(t-\tau)},\quad u_2 = (u_0)_2 \cdot e^{\lambda t},\quad u_3 = (u_0)_3 \cdot e^{\lambda t}, \tag{35}$$

Substituting into equations (32)-(34) and simplifying gives linear equations on $(u_0)_i$. The matrix of this system is

$$J = \begin{bmatrix} \lambda & 0 & \frac{c\,\mu_n}{d} - \frac{\mu_c\,a}{d} \\ -\frac{d\,\Gamma}{\gamma\,e^{(\lambda\,\tau)}} - \frac{\alpha\,c\,\mu_n}{\gamma\,a\,e^{(\lambda\,\tau)}} + \frac{\alpha\,\mu_c}{\gamma\,e^{(\lambda\,\tau)}} & \lambda & -\frac{\Gamma\,c}{\gamma} - \frac{\alpha\,c^2\,\mu_n}{\gamma\,d\,a} + \frac{\alpha\,\mu_c\,c}{\gamma\,d} \\ \frac{\mu_n\,\alpha}{a} & \frac{\mu_n\,\gamma}{a} & 0 \end{bmatrix} \tag{36}$$

The characteristic equation of this system is then the determinant of this matrix. It is given by

$$\frac{A}{a^2 e^{(\lambda\,\tau)}\,d} = 0$$

where

$$\begin{aligned} A \;=\; & -\mu_n(-\lambda\,c\,\Gamma\,d\,a - \lambda\,c^2\,\alpha\,\mu_n + \lambda\,c\,\alpha\,\mu_c\,a + \alpha\,\lambda\,a\,c\,\mu_n - \alpha\,\lambda\,a^2\,\mu_c)\,e^{(\lambda\,\tau)} \\ & -\mu_n(\Gamma\,d\,a\,c\,\mu_n - \Gamma\,d\,a^2\,\mu_c + \alpha\,c^2\,{\mu_n}^2 - 2\,\alpha\,c\,\mu_n\,\mu_c\,a + \alpha\,{\mu_c}^2\,a^2) \end{aligned} \tag{37}$$

Setting $A = 0, \lambda = 0$, and solving gives the bifurcation curves where a change in stability of the equilibria may occur. Solving for α, we obtain

$$\alpha = \frac{\Gamma\,d\,a}{-c\,\mu_n + \mu_c\,a} = \frac{\Gamma}{R_n^*} \tag{38}$$

where R_n^* is the R_n value of the endemic equilibrium.

Setting $\lambda = iw$ gives the curves along which Hopf bifurcations may occur. Expressions which the Hopf must satisfy are found in closed form solution as

$$\frac{\mu_n\cos(w\,\tau)\,(-\Gamma\,d\,a\,c\,\mu_n + \Gamma\,d\,a^2\,\mu_c - \alpha\,c^2\,{\mu_n}^2 + 2\,\alpha\,c\,\mu_n\,\mu_c\,a - \alpha\,{\mu_c}^2\,a^2)}{a^2\,d} = 0 \tag{39}$$

and

$$\frac{-\mu_n(-w\,c\,\Gamma\,d\,a - \mu_n\,w\,c^2\,\alpha + w\,c\,\alpha\,\mu_c\,a + \mu_n\,\alpha\,w\,c\,a - \alpha\,w\,\mu_c\,a^2)}{a^2 d} \tag{40}$$

$$-\frac{\mu_n\sin(w\,\tau)(-\mu_n\,\Gamma\,c\,d\,a + \Gamma\,\mu_c\,d\,a^2 - {\mu_n}^2\,\alpha\,c^2 + 2\mu_n\,\alpha\,c\,\mu_c\,a - \alpha\,{\mu_c}^2\,a^2)}{a^2\,d} = 0. \tag{41}$$

We were not able to eliminate w from the equations. If we assume the delay is small, we can Taylor expand the trigonometric terms. Ignoring terms that are $O((w\tau)^4)$ and higher, we can eliminate w to obtain the curve

$$\frac{\alpha\,(-c\,\mu_n + \mu_c\,a)\,(2\,a\,\mu_c\,\tau + 3\,a - 3\,c - 2\,c\,\mu_n\,\tau)}{\Gamma\,a\,(-3\,c - 2\,c\,\mu_n\,\tau + 2\,a\,\mu_c\,\tau)} = 0 \tag{42}$$

along which a Hopf bifurcation may occur. We observe that the curve of possible Hopf bifurcations in the model with no delay is given by

$$-\frac{(c\,\mu_n - \mu_c\,a)\,\alpha}{\Gamma\,a} = 0 \tag{43}$$

3.3 Analysis of Numerical Simulations

In an effort to obtain a better qualitative understanding of our system, OJOPLOT, a Matlab code, was written and used to numerically integrate our system of equations using 4th and 8th order Runga-Katta method. The lack of experimental data available forced us to estimate paramter values to produce somewhat realistic results. As demonstrated earlier, the dynamic behavior of the system depends largely on the value of the parameter a, and here we show evidence to support the previous statements regarding the qualitative behavior of the system.

For $a \in (0, \frac{\mu_c}{\mu_n}) = (0, a^o)$, we show all solutions should oscillate and eventually limit upon the invariant plane defined by $R_n = 0$. For any initial conditions inside this plane, trajectories will always be part of a center. Motions in these invariant planes are defined by a family of non-isolated close orbits.

For values of $a \in [\frac{\mu_c}{\mu_n}, \frac{\alpha\mu_n a}{\mu_c a}] = (a^o, a^*)$, we expect all solutions to oscillate about positive values of R_n, C, and T. It is important to emphasize that because of the nature of the steady state that results from a in this interval, no solutions should go to zero. In fact, in this section we demonstrate that all solutions must limit to a *steady limit cycle.*

For all solutions associated with $a \in (\frac{\alpha\mu_n a}{\mu_c a}, \infty) = (a^*, \infty)$, we expect all solutions to eventually limit upon the invariant plane defined by $C = 0$ (undergoing periodic oscillations as it does so). Similar to the $R_n = 0$ plane, for

Parameter	Value
Γ	1.5
α	$67/4500 \approx 0.014889$
γ	$67/1800 \approx 0.037222$
c	$1/7000 \approx 1.42847\text{x}10^{-4}$
d	$\text{d} = 1/28000 \approx 3.57243\text{x}10^{-5}$
μ_n	0.4
μ_c	$1/45 \approx 0.022222$

Figure 13: All graphs share the following initial conditions:$(R_n, C, T) = (120, 6, 200)$

initial conditions starting in this plane $C = 0$ all solutions are defined by a family of non isolated close curves.

Now, all of these qualitative descriptions will be verified numerically. In this section, we present and discuss various results for both the delay and non delay model. All following graphs have units of photoreceptors in millions and time in years. All graphs plotted against time are also normalized, using the original average number of photoreceptors in a normal individual, about 126 million[19]. The following parameters were used in all of these simulations, and only a was varied to obtain the different qualitative behavior described earlier.

We start by picking a value for a such that $a \in (0, a^o)$. In the graphs plotted against time, you can see that although cones appear to oscillate about positive values, the rod population approaches zero. This corresponds to the solutions approaching the invariant plane $R_n = 0$. Note that a small time delay has little effect.

To better illustrate this behavior, we now include a phase space portrait of the system for various intial conditions when the parameter $a \in (0, a^o)$. Here, we see that solutions are repelled from the E_3 in the plane $C = 0$, and oscillate as they approach the plane $R_n = 0$, which contains the equilibrium point E_2.

Now, we pick values of $a \in (a^o, a^*)$, where the "healthy human" equilibrium E_4 exists. Again, we expect solutions corresponding to rods and cones to oscillate about positive values, which is seen below. Once again, a small time delay has little effect.

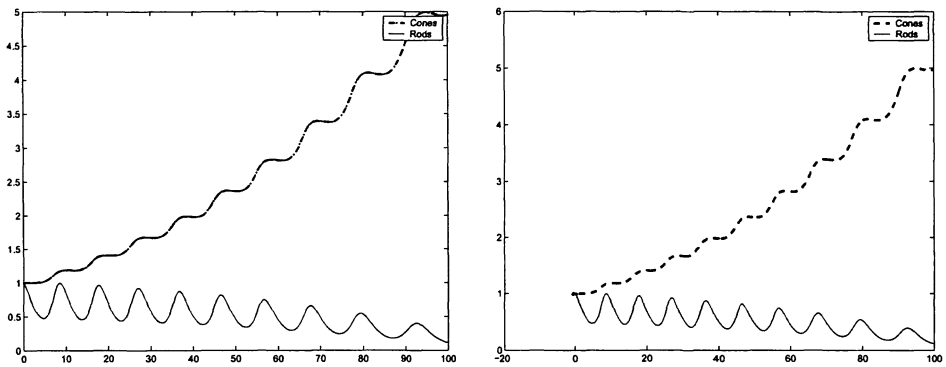

Figure 14: (a) $a = .0045, \tau = 0$ (b)$a = .0045, \tau = 1$

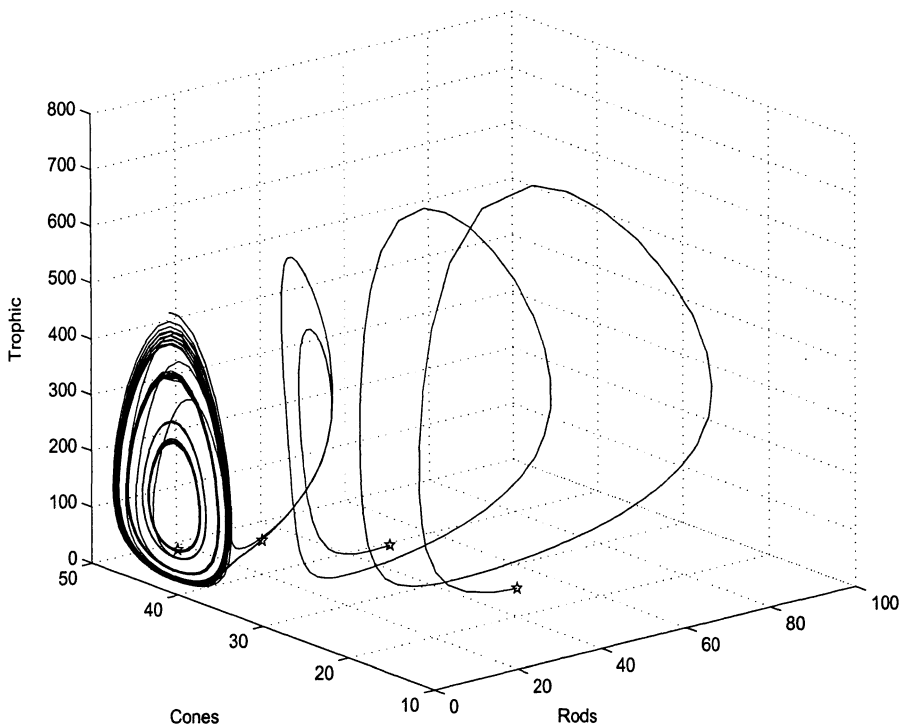

Figure 15: (a) $a \in (0, a^o), \tau = 0$ for different initial conditions

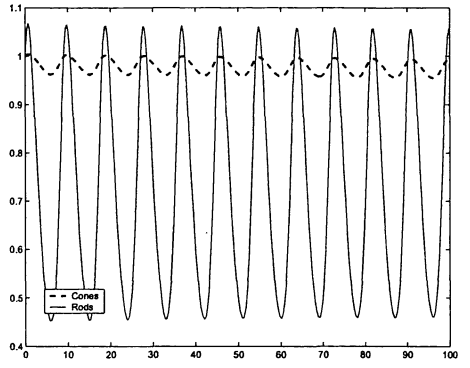

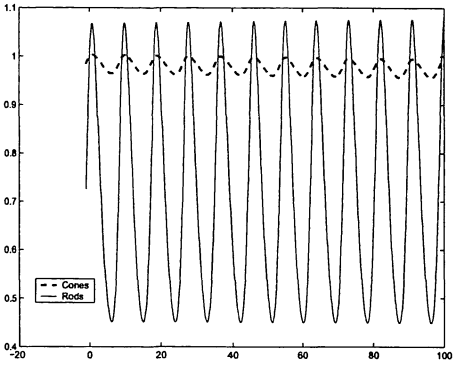

Figure 16: (a) $a = .0015, \tau = 0$ (b)$a = .0015, \tau = 1$

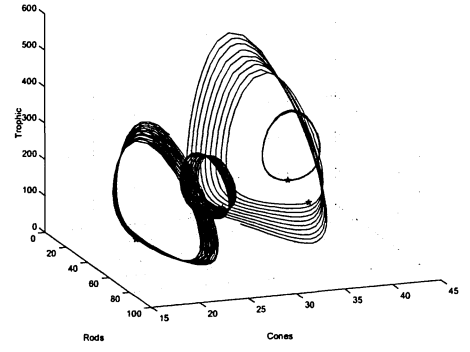

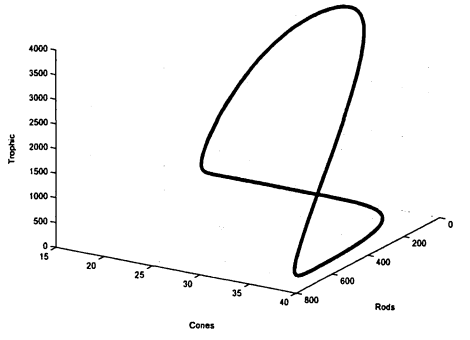

Figure 17: (a) $a = (a^0, a^*), \tau = 0$ (b)Limit cycle exists for $a = (a^0, a^*)$

Again, we show a phase space portrait with various initial conditions to show how in fact, all solutions appear to be repelled both from E_3 and E_2. We also show that a limit cycle exists by running the simulations for longer times and ignore the transient solutions, and showing that all initial conditions approach the same limit cycle.

Finally, we examine parameter values of $a \in (a^*, \infty)$. Here, E_4 no longer is biologically relevant, and the cone population should approach zero while the rods oscillate about some positive value, which is shown below. As in all previous cases, a small time delay has little effect on the qualitative behavior of the system.

Finally, we show the phase space portrait for various initial conditions.

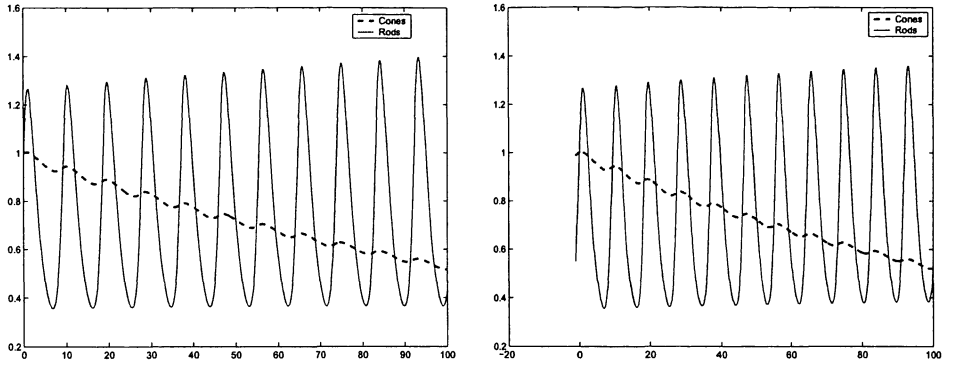

Figure 18: (a) $a = .0045, \tau = 0$ (b)$a = .0045, \tau = 1$

Here, we see that all solutions appear to be repelled by E_2 in the plane $R_n = 0$ and attracted to the point E_3 in the plane $C = 0$.

4 The disease model: Retinitis pigmentosa

We now consider what happens to the dynamics of hte rod-cone interaction wehn we introduce a retinally degernative disease such as RP. Introducing such a change adds a new dimension to our system. All variables and paramters have the same definitions and restrictions in system of equations 1. In the presence of RP the rods are divided into two groups: normal (R_n) and mutated (R_m).

$$\begin{aligned}
\dot{R_n} &= R_n(t)(aT(t) - \mu_n - m) \\
\dot{R_m} &= R_m(t)(bT(t) - \mu_m) + R_n m \\
\dot{C} &= C(t)(cT(t) - \mu_c + dR_n(t)) \\
\dot{T} &= T(t)(\Gamma - \alpha R_n(t) - \beta R_m(t) - \gamma C(t))
\end{aligned} \tag{44}$$

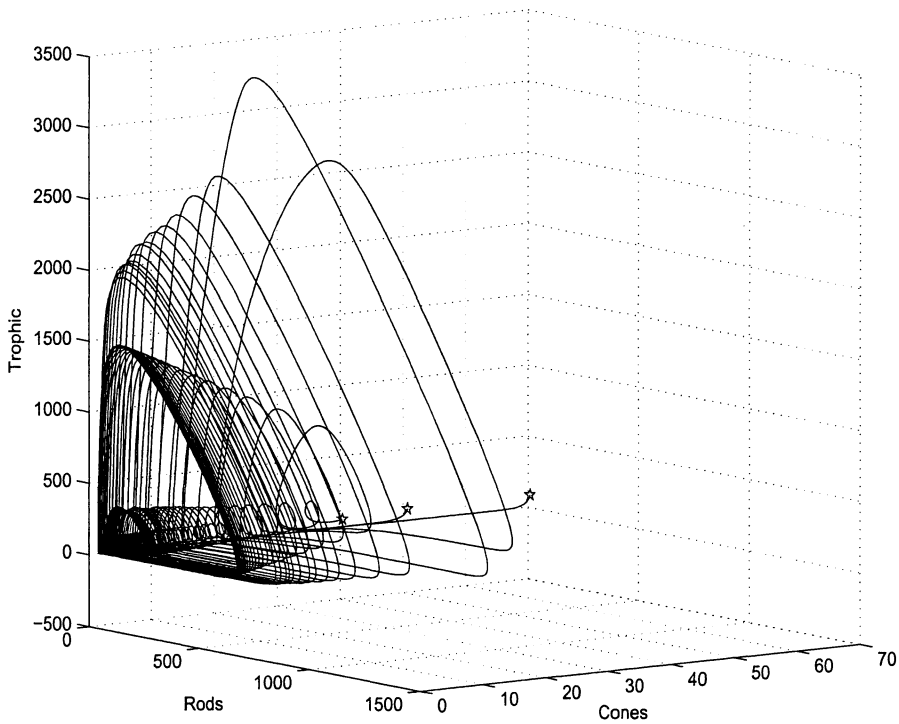

Figure 19: (a) $a = .003, \tau = 0$ (b)$a = .003, \tau = 1$

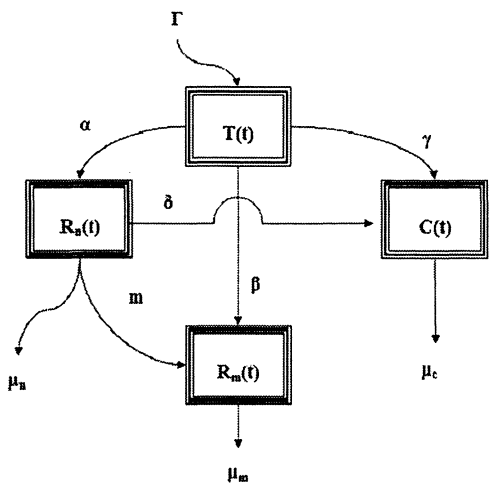

Figure 20: The model with disease.

4.1 The Model With $\tau = 0$ i.e. no delay

Incorporating delay delay does not change the equilibrium points, it only changes the a values for which the bifurcation occurs. Thus, for the remainder of this paper we shall omit τ. Equilibrium points are written in the form (R_n, R_m, C, T).

$E_1 = (0, 0, 0, 0)$ which corresponds to the origin. It always exists biologically but is never stable.

The second steady state solution $E_2 = (0, 0, \frac{\Gamma}{\gamma}, \frac{\mu_c}{c})$, is the rod free equilibrium. It always exists and is stable when $-c\mu_c - cm + mu_c a < 0$ and $(\frac{b\mu_c}{cmu_m}) < 1$

A third fixed point, $E_3 = (0, \frac{\Gamma}{\beta}, 0, \frac{\mu_m}{b})$, is the "total disease" state–so referred because only diseased rods exist. The total disease equilibrium always

exists and is stable when $-b\mu_n - bm + \mu_m a < 0$ and $(\frac{c\mu_m}{b\mu_c}) < 1$.

The fourth equilibrium point,

$$E_4 = (\frac{\Gamma(-b\mu_n - bm + a\mu_m)}{ma\beta + \alpha(-b\mu_n - bm + a\mu_m)}, \frac{\Gamma ma}{ma\beta + \alpha(-b\mu_n - bm + a\mu_m)}, 0, \frac{\mu_n + m}{a})$$

is the cone free equilibrium. It exists when $-\frac{ma\beta}{\alpha} < -b\mu_n - bm + a\mu_m$ and $-b\mu_n - bm + a\mu_m > 0$. Stability is difficult to determine.

The final equilibrium point,

$$E_5 = \left(\frac{-c\mu_n - cm + a\mu_c}{da}, \frac{(-c\mu_n - cm + a\mu_c)m}{(-b\mu_n - bm + a\mu_m)d}, \frac{\Gamma}{\gamma} - \frac{\alpha(-c\mu_n - cm + a\mu_c)(a\mu_m - bm - b\mu_n + ma\beta)}{\gamma da}, \frac{\mu_n + m}{a}\right)$$

is the endemic equilibrium. It exists when $-c\mu_n - cm + a\mu_c > 0$, $-b\mu_n - bm + a\mu_m > 0$, and $C > 0$. Stability can not be easily concluded. Eigenvalue analysis led to page long eigenvalues, and Routh-Hurwitz criteria are also lengthy and intricately conditional.

5 Preliminary Results from Numerical Simulations of R_m System

As previously stated, analyzing the system mathematically that incorporates disease is extremely difficult. Therefore, given that we had gained a small amount of insight from the simple disease-free model, we chose to consider the model containing R_m numerically as a perturbation of the simpler system without R_m. To do this, we choose similiar (though in a few cases different) parameter values and initial conditions and ran various numerical simulations using OJOPLOT2,a variation of the original code OJOPLOT use to analyze the simpler system. In this section, we present three interesting cases for consideration. While this is by no means a complete analysis, we consider these simulations in the hope of drawing possible connections between the complex model and the simple one, which we understand much better. NOTE: Since we have moved from the simple 3-D model to the more complex 4-D model, we now must consider different parameter values that were not present in

Parameter	Value
τ	0
Γ	2
α	$67/4500 \approx 0.014889$
β	0.000001
γ	$67/1800 \approx 0.037222$
a	0.003
b	0.0045
c	$1/7000 \approx 1.42847\text{x}10^{-4}$
d	$1/28000 \approx 3.57243\text{x}10^{-5}$
μ_n	0.4
μ_m	0.6
μ_c	0.025
m	0.000001

Figure 21: Initial Conditions for Case #2:$(R_n, C, T, R_m) = (120, 6, 200, 6)$

previous analysis. These parameters are μ_m, m, β, and b. For a description of these parameters, see the parameter table presented earlier in this paper.

In Case 1, the largest changes to the original parameters came in Γ. We introduced a mutation rate m, which is very small. Also, we assumed that normal rods operate better than mutant rods in their efficiency at drawing and converting trophic factor (i.e. $a > b$). Also, we assume that normal and mutant rods die at different rates (i.e. $\mu_m > \mu_n$).

When analyzing the graph, a few interesting features should be pointed out. First and foremost, for certain parameter values, the oscillatory nature of the simple model is conserved. Secondly, and perhaps more interesting, we can see that at large t values, *the cones approach zero while all other parameters continue oscillating to what appears to be a steady state.* This suggests an analog to the invariant planes in our simple 3-D model. This idea of *invariant spaces* is very interesting, and has very potentially significant applications in this disease model. If we could find solutions that lived in an invariant space in which $R_m = 0$, this could be exploited to develop strategies aimed at treating degenerative diseases that affect the photoreceptors. This idea is further explored in Cases 2 and 3.

The differences between Case 1 and Case 2 include changes in Γ and d. Also, by increasing μ_c we assume that cones die at a higher rate in the

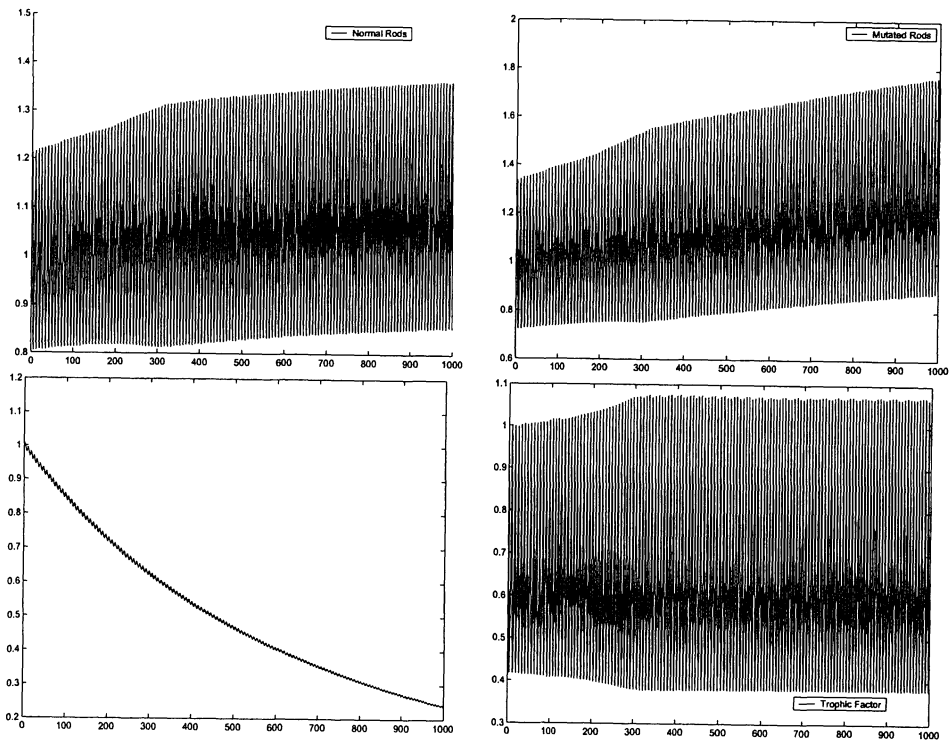

Case 22: (a) Normal Rods (b)Mutant Rods (c) Cones (d)Trophic Factor

Parameter	Value
τ	0
Γ	1
α	$67/4500 \approx 0.014889$
β	0.000001
γ	$67/1800 \approx 0.037222$
a	0.005
b	0.0045
c	$1/7000 \approx 1.42847\text{x}10^{-4}$
d	$1/2000 = 0.0005$
μ_n	0.4
μ_m	0.4
μ_c	$1/30 \approx 0.0333$
m	0.000001

Figure 23: Initial Conditions for Case #2:$(R_n, C, T, R_m) = (120, 6, 200, 6)$

presence of mutant rods than in normal ones. Finally, we assume that normal and mutant rods die at the same rate ($\mu_m = \mu_n$) and draw from and convert trophic factor at similiar rates ($a \approx b$).

It is immediately clear that Case 2 shows a solution that tends towards an invariant space in which $R_m = 0$. All other variables continue to oscillate and appear to approach a steady state that is much higher than their initial amounts. This is interesting, because it contrasts somewhat with the results obtained in Case 3, as we will see shortly.

The differences between Case 2 and Case 3 include: Γ is increased, and it is assumed that rods are aiding cones less (d is reduced). Finally, the death rate for the cones is increased (the negative effect of mutated rods on the survival of the cones is assumed to be stronger here than in Case 2).

Like Case 2, Case 3 appears to live in an invariant space with $R_m = 0$. However, the qualitative dynamics of the cone population are much different. Instead of oscillating upwards to reach a steady state, it now appears as if cones are oscillating to reach a steady state that was lower than its original value and definitely less than the steady state achieved by the cones of Case 2.

From these three simulations, we were able to observe the oscillatory and invariant space nature of this new complex system. The changes in parame-

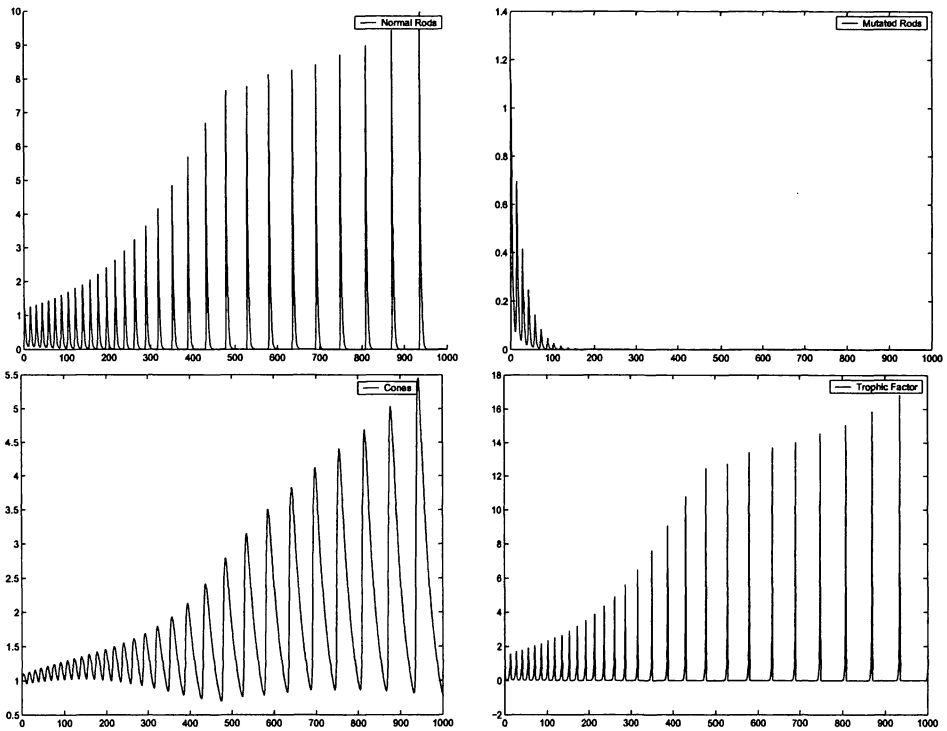

Case 24: (a) Normal Rods (b)Mutant Rods (c) Cones (d)Trophic Factor

Parameter	Value
τ	0
Γ	1.5
α	$67/4500 \approx 0.014889$
β	0.000001
γ	$67/1800 \approx 0.037222$
a	0.005
b	0.0045
c	$1/7000 \approx 1.42847\text{x}10^{-4}$
d	$1/2500 = 0.0004$
μ_n	0.4
μ_m	0.4
μ_c	0.05
m	0.000001

Figure 25: Initial Conditions for Case #3:$(R_n, C, T, R_m) = (120, 6, 200, 6)$

ters made in these three cases also suggest that Γ may play an imporant role in determining the dynamics of the new system. We also hypothesize that many of the other properites of the simple system are conserved in the more complex one, and future work should focus on determining whether or not these exist. We are particularly interested in investigating the existence of the analog to the critical interval for the parameter a in the simple model.

6 Conclusion

Mathematical investigation into the nature of direct and indirect interactions between photoreceptors has provided an interesting and insightful system. The first and most important conclusion to be drawn is that there *must* exist a direct cell-cell interaction via horizontal cells and gap junctions through which rods communicate with cones. By removing this interaction, we found that the system reduced to a two predator-single prey system in which rod-cone coexistence is impossible. Independent of initial conditions, the rods or cones will eventually go extinct in the absence of this direct interaction term. This is biologically impossible (since healthy people have both rods and cones) and indicates there must exist a direct interaction. There may be, however, other important interactions not accounted for in this model.

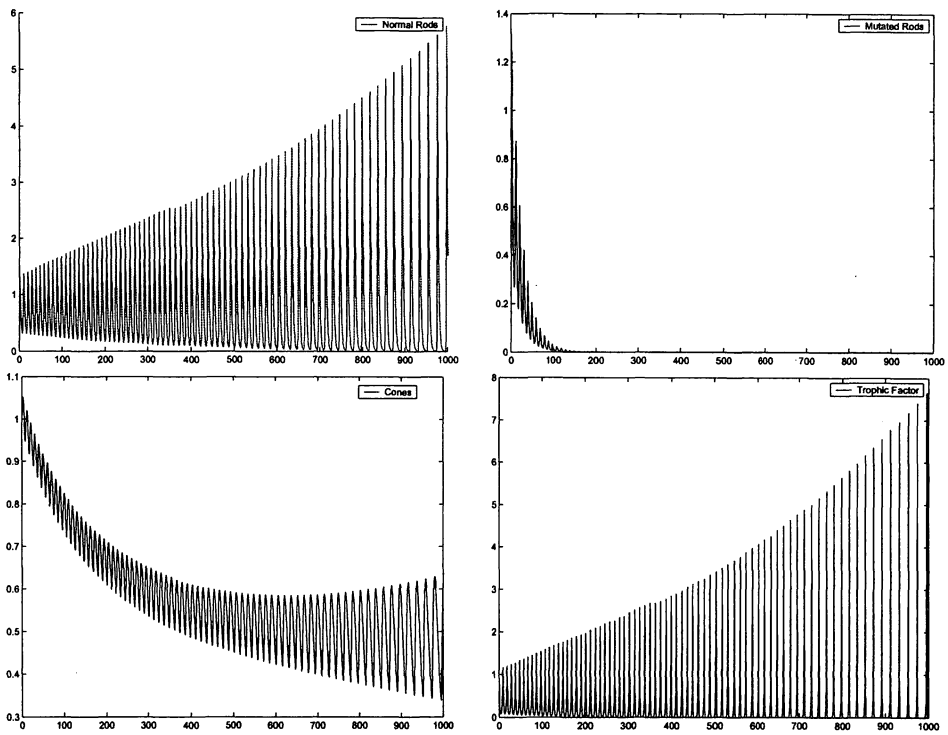

Case 26: (a) Normal Rods (b)Mutant Rods (c) Cones (d)Trophic Factor

Next, we were able to show the importance of α in the system. Recall that α is the per cell rate at which normal rods draw from the trophic pool. While α was in a particular interval the healthy human equilibrium existed, and for α outside of this interval various initial conditions always limited on invariant planes. One bound on this interval was a function of Γ, thus developing treatments that affect the influx rate into the trophic pool could have applications to decellerating natural vision loss in healthy individuals. Vitamin A, for example, has been shown to have positive effects in slowing retinal degeneration.[8] It is quite likely that Vitamin A is a component of the trophic pool.

Our abbreviated investigation into the effect of time delay showed it to have little effect on our system. When considering terms containing $e^{\lambda I \tau}$ in the characteristic equation, we Taylor expanded the corresponding trigonometric functions. The expansion led to an approximation valid only for small delays since we ignored higher order terms. The end effect of the small time delay was to alter the values for which the healthy human equilibria biologically existed. While this does have biological value (prolonging existence of the healthy human equilibrium point) it had no other effect. Further investigation is needed to rule out other effects of time delay, and a better implementation allowing for more accurate estimations at higher values is needed.

We are excited by the rich dynamics of a deceptively simple system, and much more work is needed to understand this system and its variations more completely. The investigation of two independent trophic factor pools for rods and cones respectively, or investigation into the toxicity hypothesis could prove useful. The diseased system should be analyzed under the effects of direct interaction removal, or conversely an increase in trophic factor with the hope of finding a critical value for preventing secondary cone death. In all cases, more accurate estimation of parameters is needed, and for this we await the work of the biologists.

7 Acknowledgements

We would like to thank our advisors Steve Wirkus and Erika Camacho for pushing us to within ϵ of excellence. This project would not have been possible without their guidance and encouragement. We would also like to thank Carlos Castillo-Chavez for giving us the opportunity to enjoy an enlightening and truly memorable summer; the NSF, who's funding makes this and other research experiences possible; and CNLS for providing with access to their vast intellectual and computing resources which allowed us to broaden out intellectual horizons. We would also like to thank the following people and entities: OJOPLOT, Coffee, Rod Stewart, The Coneheads, our fellow MTBI students, The Waitress (Jessica), Cookies, Messenger and Wireless Networks, Carrots, Pinky and the Brain, and of course Steve's Car and yellow poles.

References

[1] Alexander D. Bazykin *Nonlinear dynamics of interacting populations.* World Scientific, New Jersey, 1998.

[2] Adam S. Berger, MD, Tongalp H. Tezel, MD, Lucian V. Del Priore, MD, PhD, and Henry J. Kaplan, MD *Photoreceptor transplantation in retinitis pigmentosa.* American Academy of Opthalmology, 110(2):383-391, 2003.

[3] Fred Brauer and Carlos Castillo-Chavez *Mathematical Models in Population Biology and Epidemiology.* Springer, New York, New York, 2001.

[4] Leah Edelstein-Keshet *Mathematical models in biology.* McGraw Hill, San Fransisco, California, 1988.

[5] Nisha Gupta, Kimberly E. Brown, and Ann H. Milam *Activated microglia in huma retinitis pigmentosa, late-onset retinal degeneration, and age-related macular degneration.* Experimental Eye Research, 76:463-471, 2003.

[6] Patti C. Huang, Alicia E. Gaitan, Ying Hao, Robert M. Petters, and Fulton Wong *Cellular interactions implicated in the mechanism of photoreceptor degeneration in transgenic mice expressing a mutant rhodopsin gene.* Proceedings of the National Academy of Sciences of the United States of America, 90(18):8484-8488, 1993.

[7] Jens Kleiner *Where vision begins-phototransduction in rods and cones.* 2001.

[8] Helga Kolb, Eduardo Fernandez, and Ralph Nelson *Webvision:organization of the retina and visual system.* http://www.webvision.med.utah.edu/ University of Utah, Utah. All figures reproduced courtesy of Helga Kolb.

[9] Yuri A. Kuznetsov *Elements of Applied Bifurcation Theory.* Springer Verlag, New York, New York, 1995.

[10] Ann H. Milam, Zong-Yi Li, and Robert N. Farris *Histopathology of Human Tapetoretinal Degenerations* Harvard, Massachusetts. http://www.djo.harvard.edu/meei/OA/MILAM/INDEX.html

[11] Retina International: Retinitis Pigmentosa. http://www.retina-international.org/rp.html

[12] Saddek Mohand-Said,David Hicks, Theirry Léveillard, Serge Picaud, Fernanda Porto, and José A. Sahel *Rod-cone interactions: developmental and clinical significance.* Progress in Retinal and Eye Research, 20(4):451-467, 2001.

[13] Clyde W. Oyster *The human eye: structure and function.* Sinauer Associates, Inc. , Sunderland, Massachusetts, 1999.

[14] Lawrence Perko *Differential equations and dynamical systems.* Springer-Verlag, New York, New York, 1996.

[15] Harris Ripps *Cell death in retinitis pigmentosa: gap junctions and the 'bystander' effect.* Experimental Eye Research, 74:327-336, 2002.

[16] Lauralee Sherwood *Human Physiology: From Cells to Systems, 4th edition.* Brooks and Cole Publishers, 2001.

[17] http://starklab.slu.edu/signal/RPAMD.html

[18] http://www-groups.dcs.st-and.ac.uk/ history/Quotations/Galileo.html School of Mathematics and Statistics, University of St. Andrews, Scotland.

[19] L. Van Warren *The Input and Output Bandwidth of the Eye and Body* http://www.wdv.com/EyeBandwidth/index.html